Achille Giacometti

Self-Assembly mechanism in proteins and nanocollids

Chiara Poletto
ISI Foundation

Amos Maritan,
Antonio Trovato
Università di Padova

Jayanth Banavar
PennState University

Artem Badasyan
Università Ca' Foscari Venezia

Fred Lado
North Carolina State University
Julio Largo
Universidad de Cantabria
Giorgio Pastore
Università di Trieste
Francesco Sciortino
Università la Sapienza di Roma

Financial support by PRIN –COFIN 2007

Conference on Nucleation, Aggregation and Growth, Bangalore 26-30 July 2010

Achille Giacometti

Self-Assembly mechanism in proteins and nanocollids

Chiara Poletto
ISI Foundation

Amos Maritan,
Antonio Trovato
Università di Padova

Jayanth Banavar
PennState University

Artem Badasyan
Università Ca' Foscari Venezia

Fred Lado
North Carolina State University
Julio Largo
Universidad de Cantabria
Giorgio Pastore
Università di Trieste
Francesco Sciortino
Università la Sapienza di Roma

Financial support by PRIN –COFIN 2007

Conference on Nucleation, Aggregation and Growth, Bangalore 26-30 July 2010

Achille Giacometti

Self-Assembly mechanism in patchy colloids

Giorgio Pastore
Università di Trieste
Francesco Sciortino
Università la Sapienza di Roma

Fred Lado
North Carolina State University
Julio Largo
Universidad de Cantabria

Financial support by PRIN –COFIN 2007

Sciortino, Giacometti, Pastore, PRL 103, 237801 (2009)

Sciortino, Giacometti, Pastore, PCCP in press (2010)

Giacometti, Lado, Largo, Pastore, Sciortino JCP 131, 174114 (2009)

Giacometti, Lado, Largo, Pastore, Sciortino JCP 132 174110 (2010)

Conference on Nucleation, Aggregation and Growth, Bangalore 26-30 July 2010

UNIVERSITÀ CA' FOSCARI VENEZIA

Outline

- The Janus paradigm
- Patchy colloids
- Integral equation theory
- Phase diagrams
- Outlook

Partial list of recent papers

Janus experimental

•Chen, Shah, Abate, Weitz, Langmuir 25, 4320 (2009)
•Wang, Li, Zhao, Li, JACS 130, 11594 (2008)
•Roh,Martin, Lahann, Nat. Mat. 4, 759 (2005)
•Erhardt et al, Macromolecules 34, 1063 (2001)
•….

Janus theory (+exp)

•Miller and Cacciuto, PRE 80, 021404 (2009)
•Hong, Cacciuto, Luijten, Granick, Langmuir 24, 621 (2008)
•Hong, Cacciuto, Luijten, Granick, NanoLett. 6, 2510 (2006)
•Vanakaras, Langmuir 22, 88 (2006)
•Jackson, Meyerson, Stellacci, Nat. Mat. 3, 330 (2004)
•Erdmann, Kroger, Hes, PRE 67, 041209 (2003)
•….

Patchy and self-assembly

•Noya, Vega, Doye, Louis, JCP 132, 234511 (2010)
•Bianchi, Largo, Tartaglia, Zaccarelli, Sciortino PRL 97, 168301 (2006)
•Cho, Yi, Lim, Kim, Manoharan, Pine, Yang, JACS 127, 15968 (2005)
•Zhang, Glotzer Nano Lett. 4, 1407 (2004)
•Jackson, Meyerson, Stellacci, Nat. Mat. 3, 330 (2004)
•Manoharan, Elsesser, Pine, Science 3010, 483 (2003)
•……

Reviews

•Pawar, Kretzschmar, Macromol. Rap. Comm. 31 150 (2010)
• Granick, Jiang, Chen, Phys. Today (July) 68,(2009)
•Walther, Muller, Soft Matter 4, 663 (2008)
•Glotzer, Solomon, Nat. Mat. 6, 557, (2007)
•….

Motivations

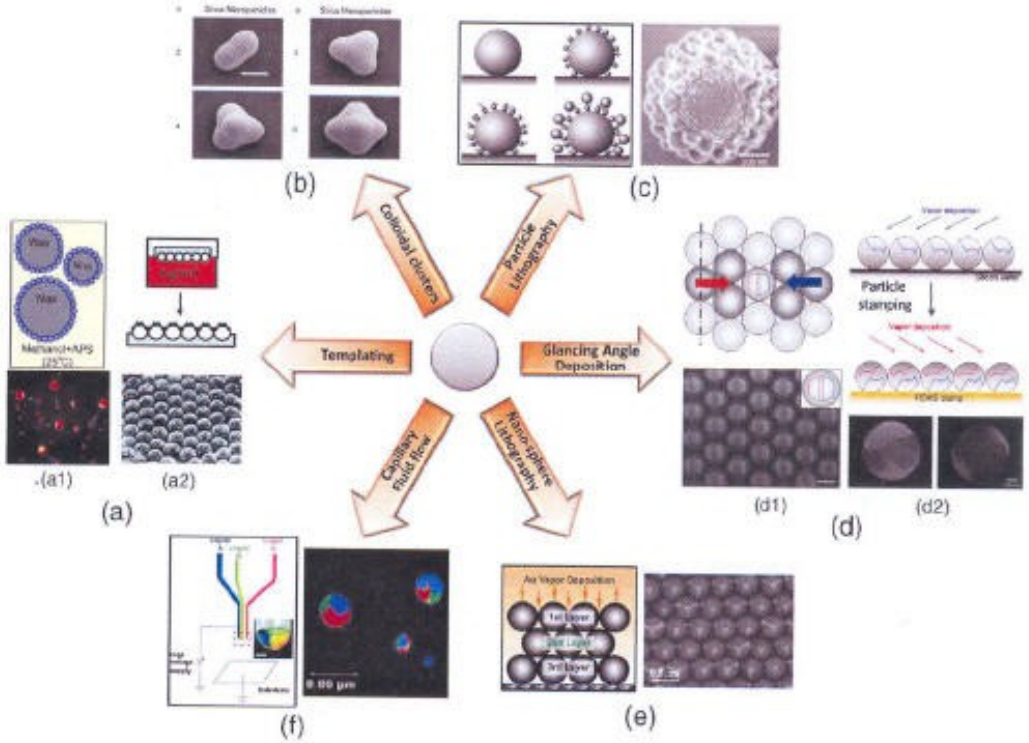

Pawar, Kretzschmar, Macrom. Rapid Commun. 31, 150 (2010)

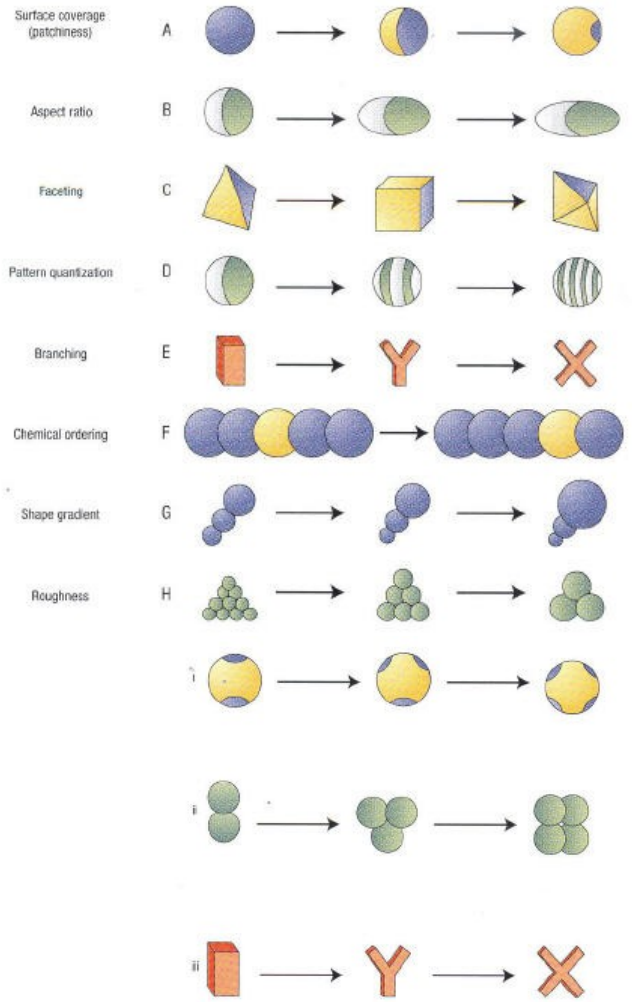

Glotzer, Solomon, Nature Materials 6, 557 (2007)

Experimental framework

Hong, Cacciuto, Luijten, Granick
Langmuir 24, 621 (2008)

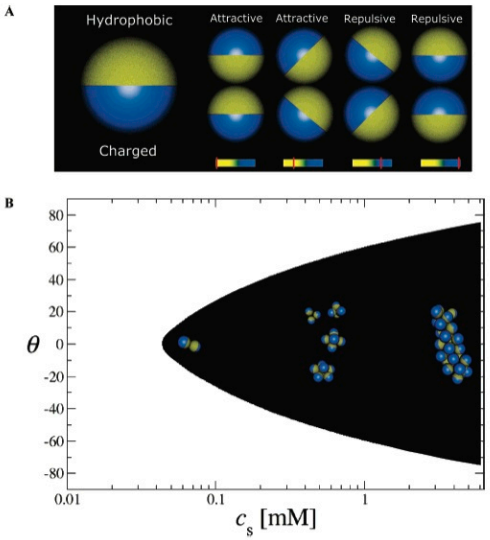

Figure 1. (A) Pairs of colloidal particles in water, each hydrophobic on one hemisphere and charged on the other (denoted by yellow and blue colors), are considered at fixed separation. The interaction potential switches from attractive when the hydrophobic sides face one another (left) to repulsive when the charged sides face one another (right), with intermediate attraction or repulsion at canted angles (middle). Below each particle pair, the intensity of the interaction potential at that mutual orientation is shown schematically. (B) Region of permitted tilt angles between two charged hemispheres with 1 μm diameter held at a center-to-center distance of 1.020 micrometers, plotted as a function of the logarithmic concentration of monovalent salt. The boundary is determined by requiring the electrostatic energy cost per simultaneous rotation of the particles over an angle θ to be smaller than 1 k_BT. The reference angle θ = 0 refers to the leftmost pair in the top panel, where the hydrophobic hemispheres face one another. The structures within the bottom panel illustrate the range of structures considered in more detail in Figures 3 and 4.

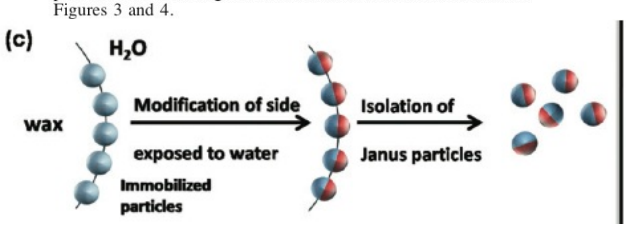

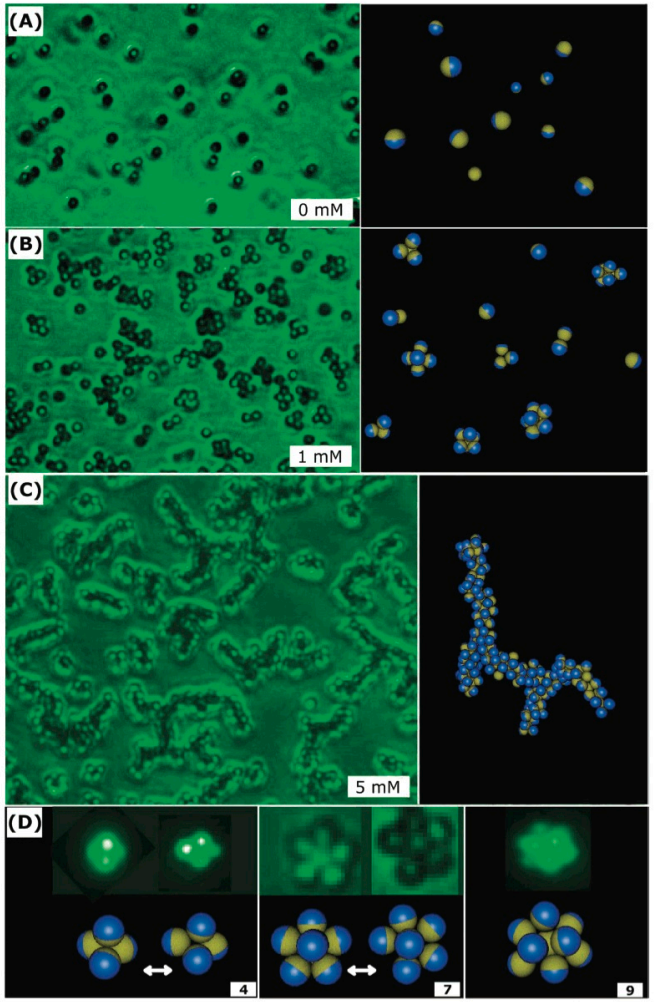

Figure 3. Varying the salt concentration causes amphiphilic particles (1 μm diameter) to assemble into clusters of various sizes and shapes. The images with green background represent epifluorescence experiments. In the Monte Carlo computer simulations, blue and yellow colors represent charged and hydrophobic hemispheres, respectively. Panel (A) shows discrete particles for the case of particles in deionized water. Panel (B) (1 mM KNO_3) shows small clusters (up to nonahedra) in equilibrium with one another. Panel (C) (5 mM KNO_3) shows long, branched wormlike strings. The simulations (right) confirm that the assembly of small clusters into strings occurs as the range of the electrostatic repulsion, relative to hydrophobic attraction, decreases with increasing salt. Panel (D) shows further comparison of epifluorescence images and Monte Carlo simulations with excellent agreement. Experimentally, clusters with the same number of particles (N) interconvert dynamically between different shapes, as confirmed from simulations for tetramers, N = 4 (left), and heptamers, N = 7 (middle). The nonahedral structure, N = 9, is also confirmed (right).

Walther, Muller, Soft Matter 4, 663 (2008)

The Kern-Frenkel model

Janus particles

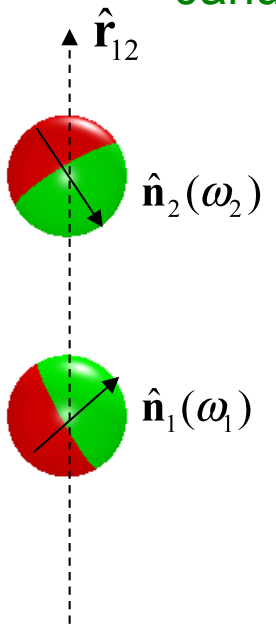

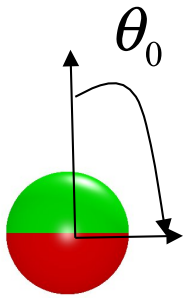

Chapman, Jackson, Gubbins
Molec. Phys. 65, 1057 (1988)
Kern, Frenkel, JCP 118, 9882 (2003)

$$\Phi(12) = \phi(r_{12})\Psi(\hat{\mathbf{n}}_1, \hat{\mathbf{n}}_2, \hat{\mathbf{r}}_{12})$$

$$\Psi(\hat{\mathbf{n}}_1, \hat{\mathbf{n}}_2, \hat{\mathbf{r}}_{12}) = \begin{cases} 1 & \hat{\mathbf{n}}_1 \cdot \hat{\mathbf{r}}_{12} \geq \cos\theta_0, \text{and}, \hat{\mathbf{n}}_2 \cdot \hat{\mathbf{r}}_{21} \geq \cos\theta_0 \\ 0 & \text{otherwise} \end{cases}$$

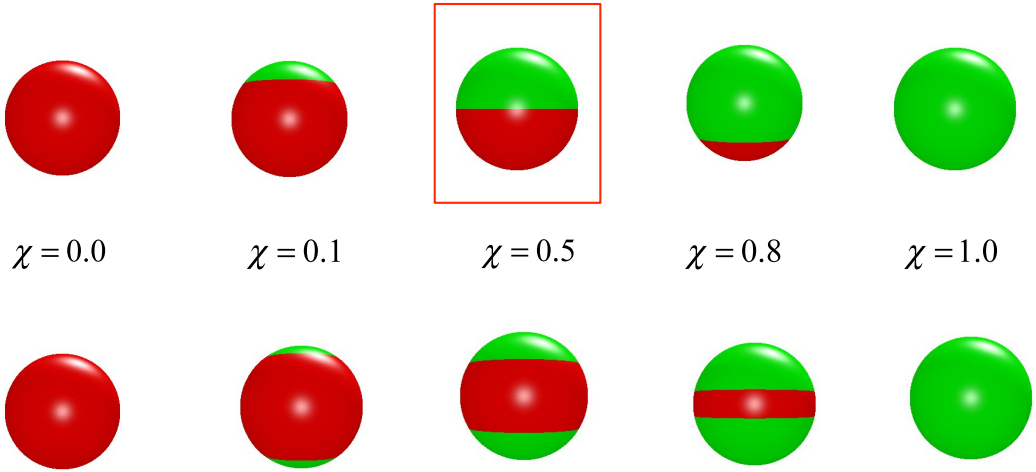

1P

2P

Square well

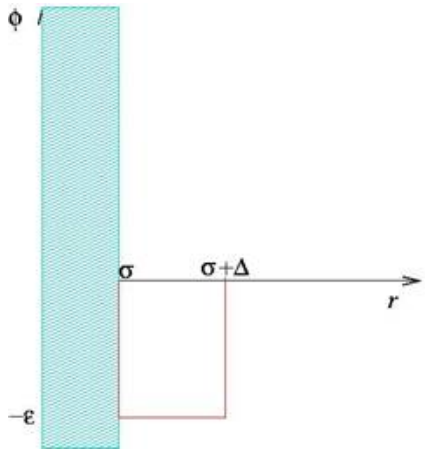

Standard colloidal phase diagram

Lennard-Jones

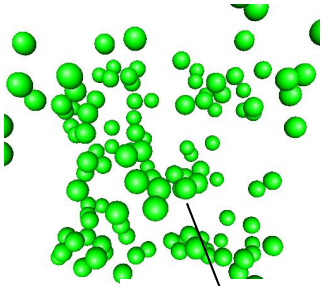

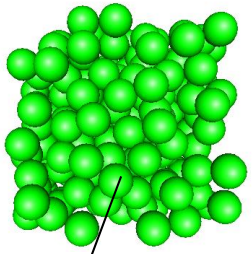

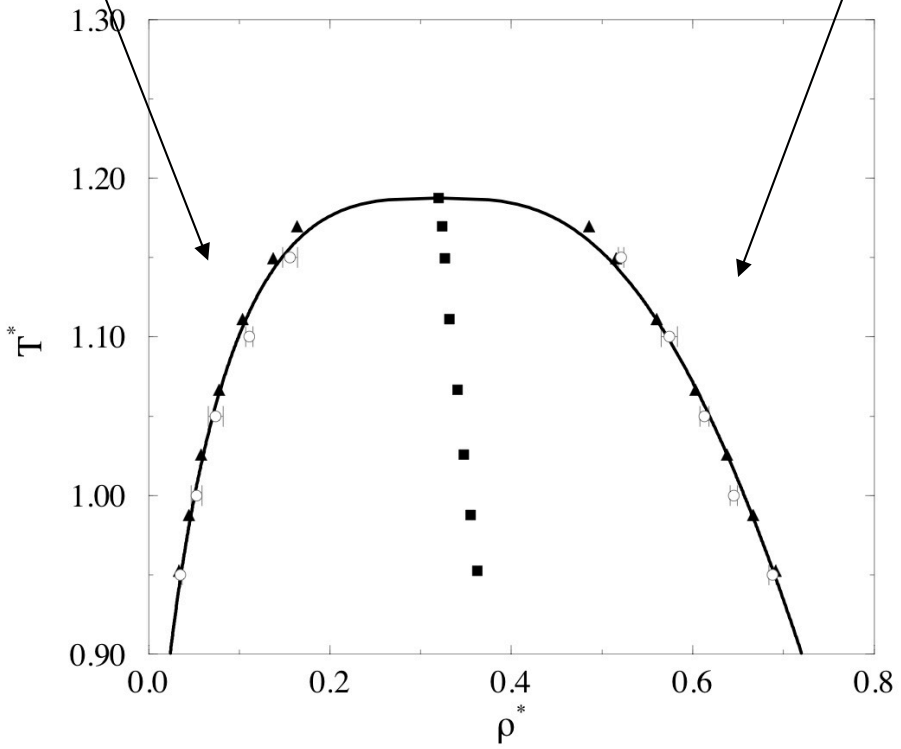

Square-well potential

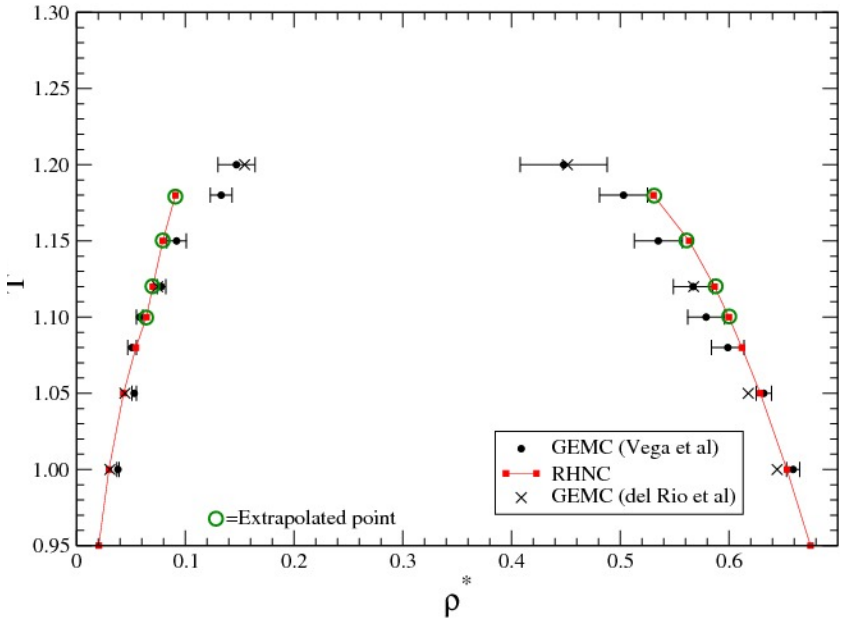

Wilding, Phys. Rev. E 52, 602 (1995)

Giacometti, Lado, Pastore, Molec. Phys. 107, 555 (2009)

UNIVERSITÀ CA' FOSCARI VENEZIA

Competing mechanism

$T^* = 0.25$

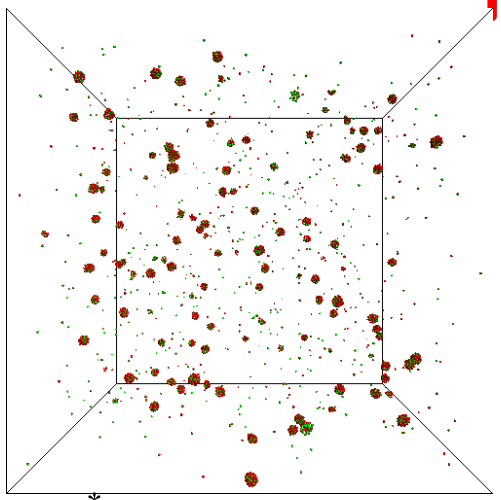

$\rho^* = 0.001$

ρ^*

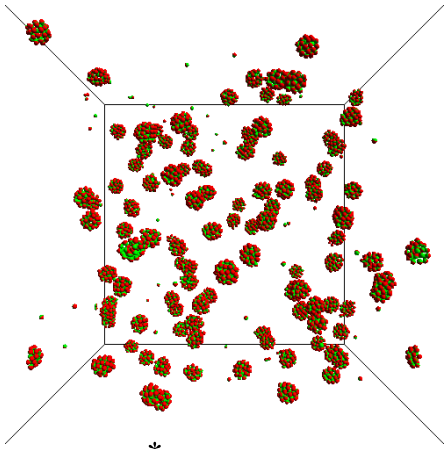

$\rho^* = 0.01$

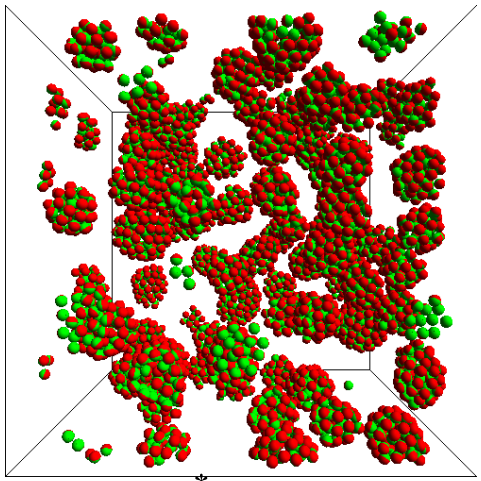

$\rho^* = 0.1$

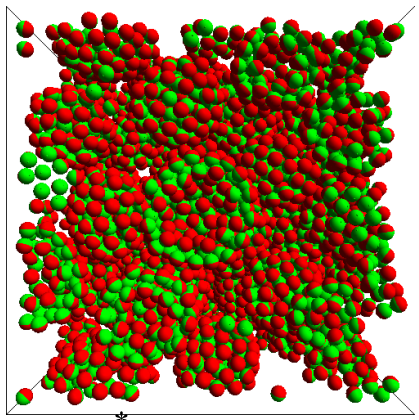

$\rho^* = 0.4$

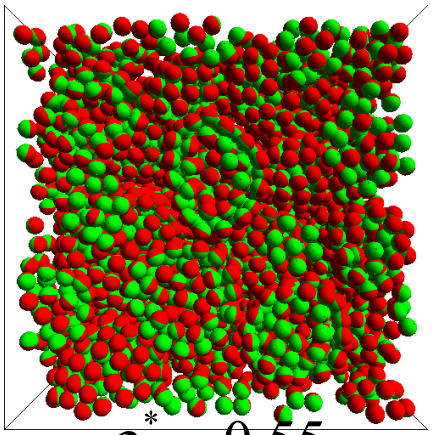

$\rho^* = 0.55$

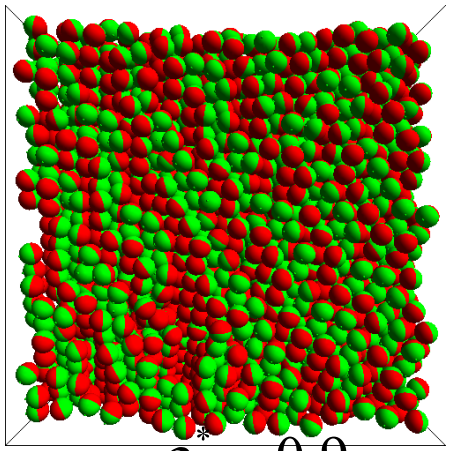

$\rho^* = 0.9$

Sciortino, Giacometti, Pastore, PRL 103, 237801 (2009)

Janus Phase diagram

Sciortino, Giacometti, Pastore, PRL 103, 237801 (2009)

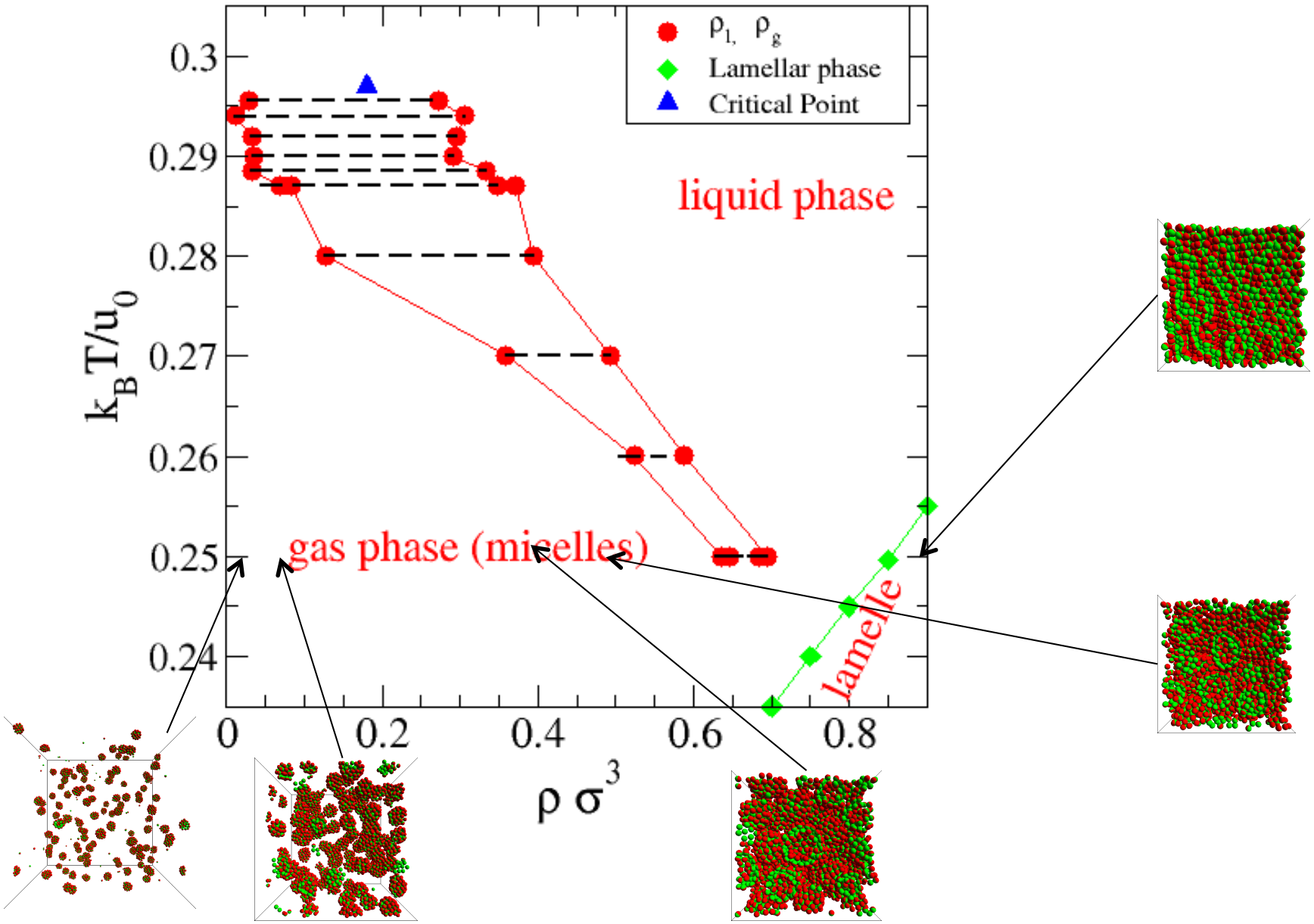

From SW to Janus

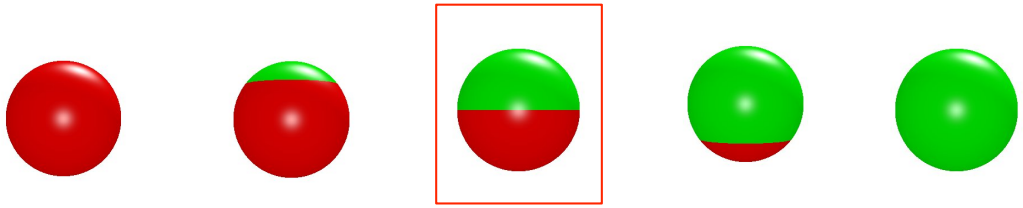

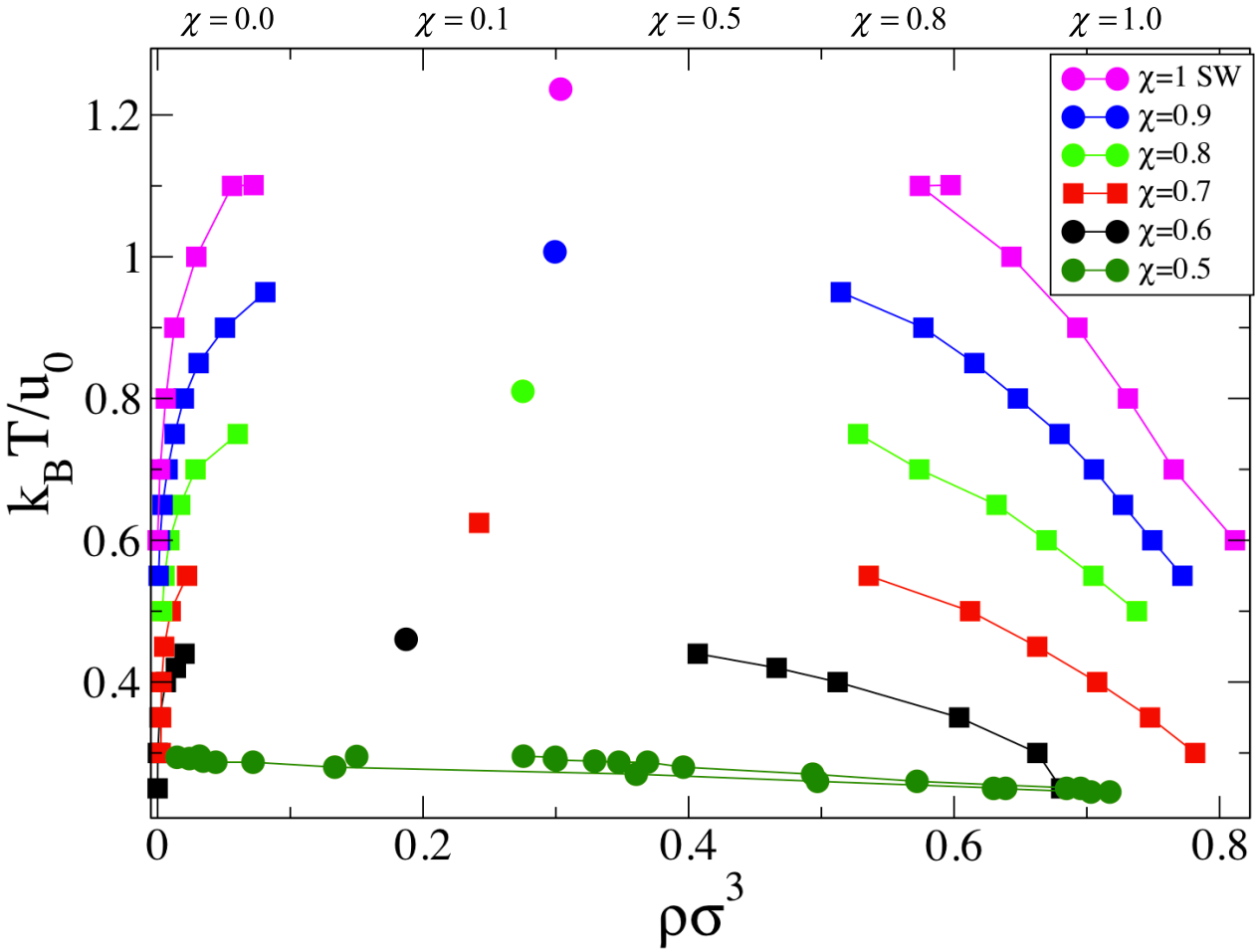

Sciortino, Giacometti, Pastore PCCP in press (2010)

Integral equation solution spherical potentials

$$h(r) = c(r) + \rho \int d^3 r' c(|\mathbf{r} - \mathbf{r}'|) h(r')$$ Exact OZ equation

$$c(r) = \exp[-\beta\phi(r) + \gamma(r) + B(r)] - 1 - \gamma(r)$$ Approximate closure

$$\gamma(r) = h(r) - c(r) \qquad g(r) = h(r) + 1$$ Auxiliary functions

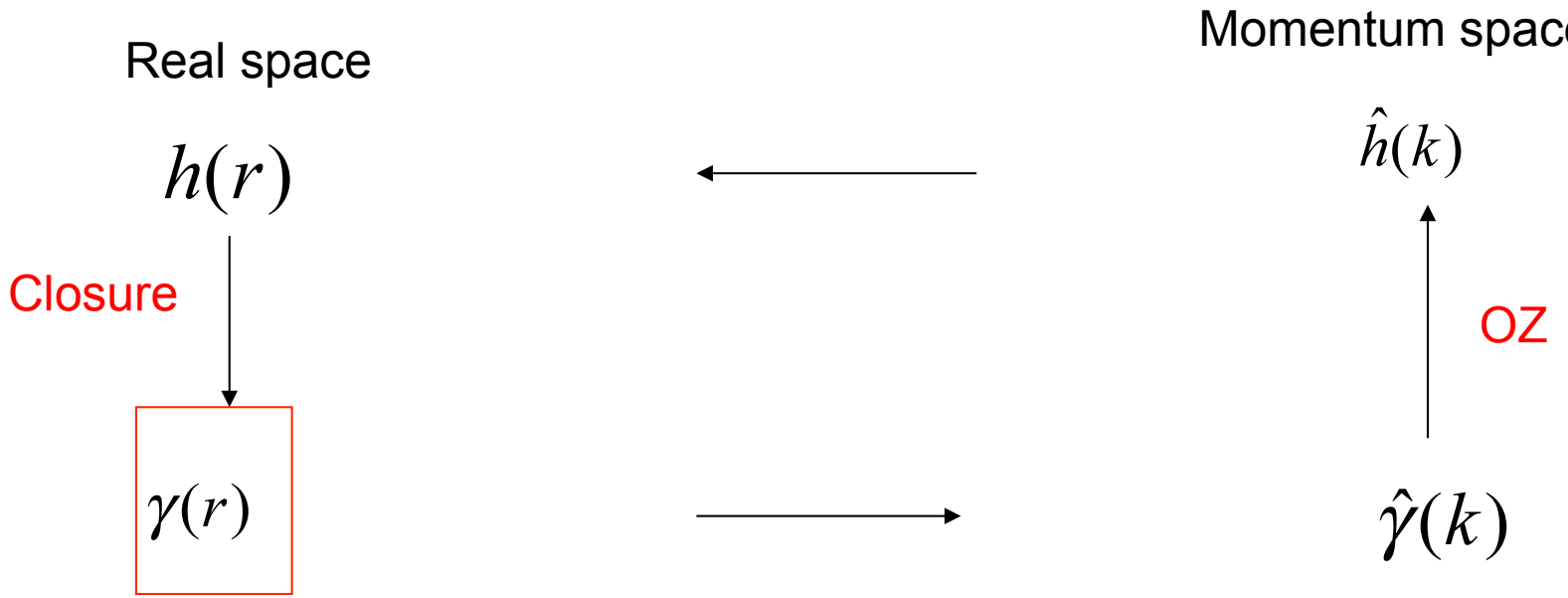

Example: RHNC for SW

$B(r)$ HS+variational optimization

$\lambda = 1.25$

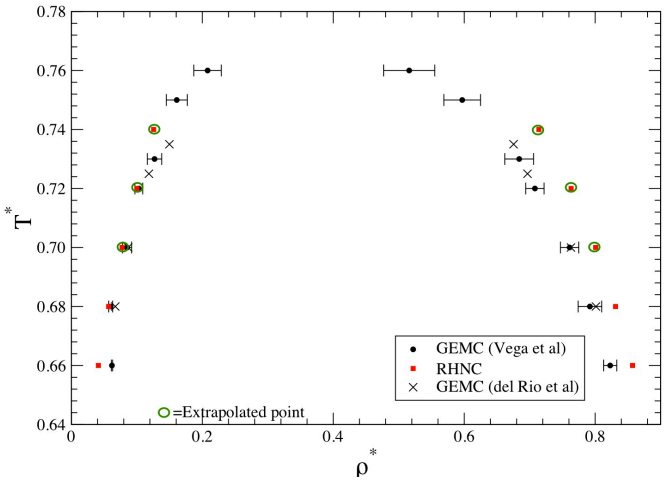

$\lambda = 1.5$

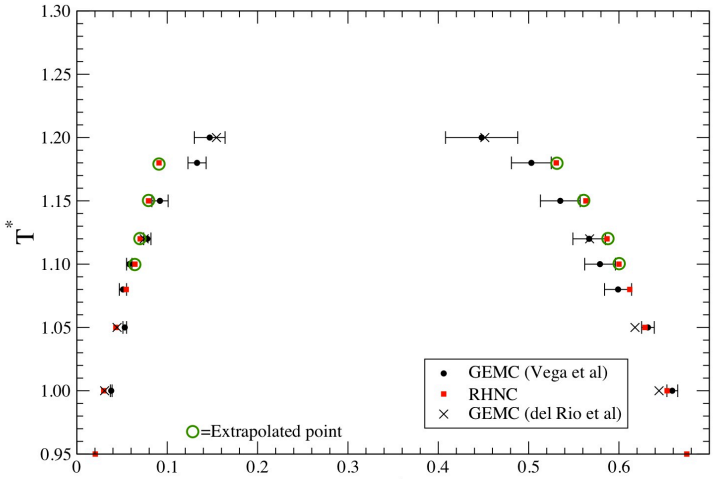

$\lambda = 1.75$

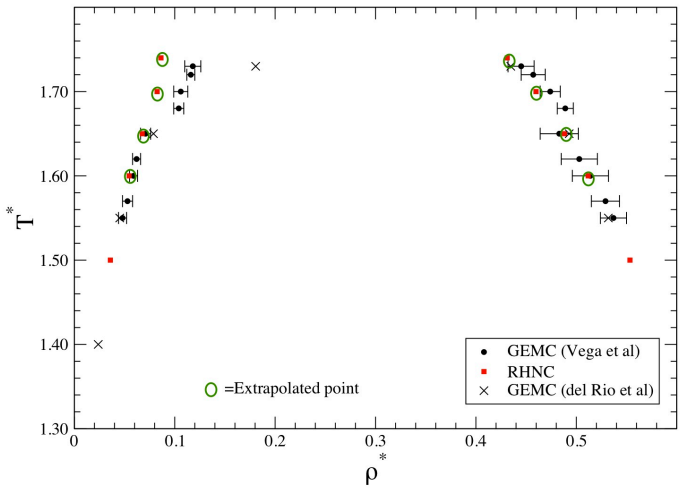

$\lambda = 2.0$

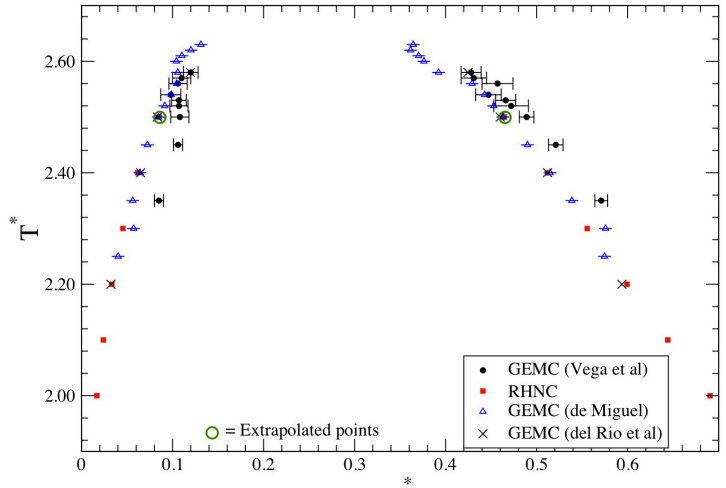

Lado, PRA 8 2548 (1973)

Roselfeld and Ashcroft, PRA 20,1208 (1979)

Whiite Lipson, Mol. Phys. 105,1983 (2007) El Mendoub, Wax, Charpentier, Jakse, Mol. Phys 106, 2667 (2008).

Schliper, Telo da Gama, Ferreira, JCP 98, 1534 (1993) Giacometti, Pastore, Lado Molec. Phys 107, 555 (2009)

Integral equation with angular dependent potentials

Much more involved!

$$h(12) = c(12) + \frac{\rho}{4\pi}\int d^3 r_3 d\omega_3 c(13) h(32)$$ OZ (exact)

$$c(12) = \exp[-\beta\Phi(12) + \gamma(12) + B(12)] - 1 - \gamma(12)$$ Closure

Expansion in spherical harmonics (general frame)

$$X(\mathbf{r}_{12}, \hat{\mathbf{n}}_1, \hat{\mathbf{n}}_2) = \sum_{l_1 l_2 l} \sum_{m_1 m_2 m} X(l_1 l_2 l, r) C(l_1 l_2 l, m_1 m_2 m) Y_{l_1 m_1}(\omega_1) Y_{l_2 m_2}(\omega_2) Y_{lm}^{*}(\Omega)$$

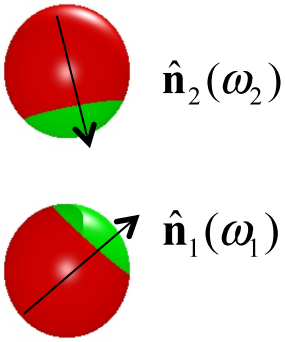

$\hat{\mathbf{z}} = \hat{\mathbf{r}}_{12}(\Omega)$ Axial frame

$\hat{\mathbf{z}} = \hat{\mathbf{k}}$ k-frame

Lado Molec. Phys. 47, 283 (1982); 299 (1982)

Flow chart for angular dependent potentials

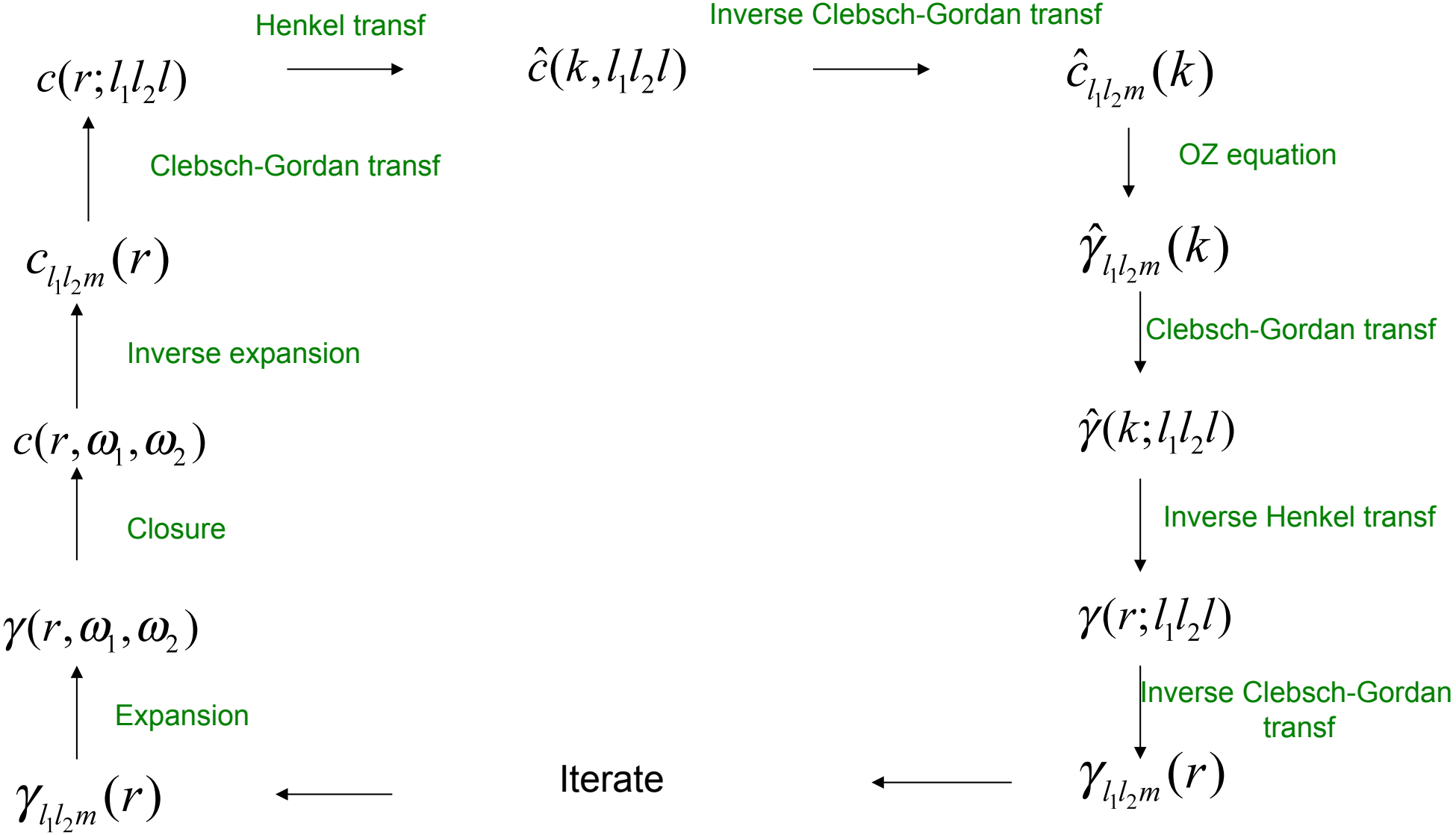

Phase diagram 1P

$\chi = 0.8$

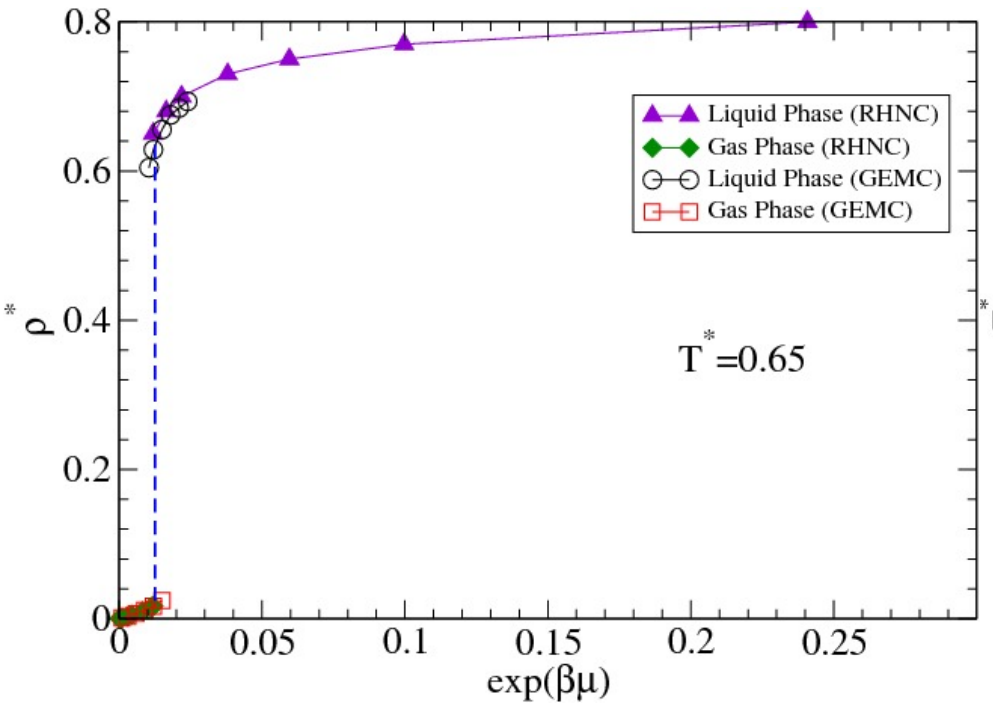

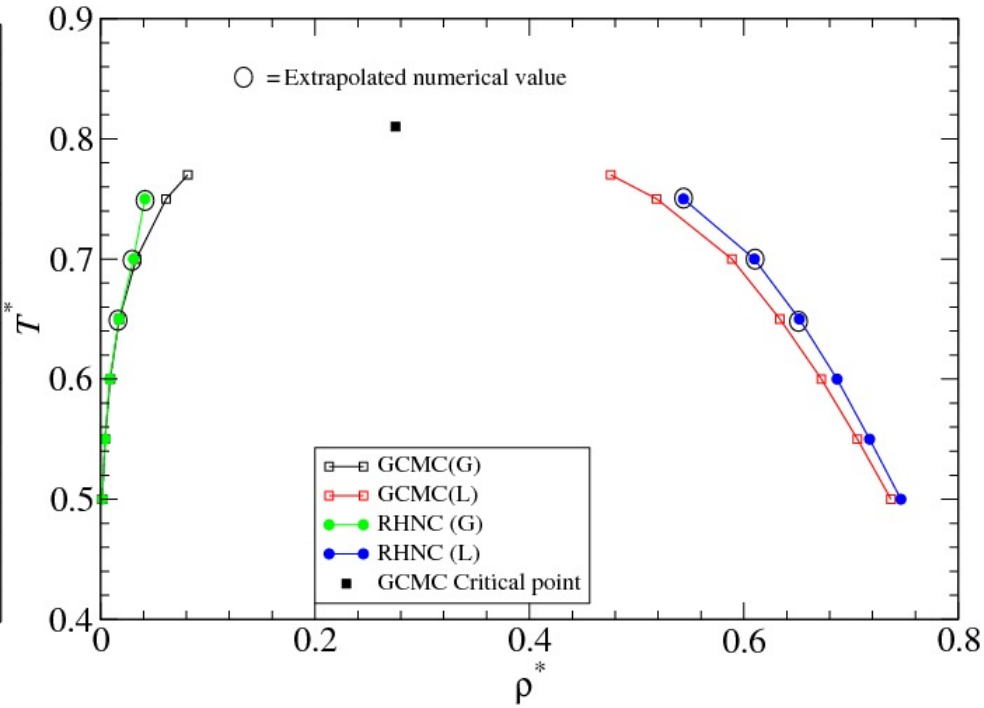

Giacometti, Lado, Largo, Pastore, Sciortino JCP 131, 174114 (2009)

Phase diagram 2P

N. Kern and D. Frenkel

Kern, Frenkel, JCP 118, 9882 (2003)

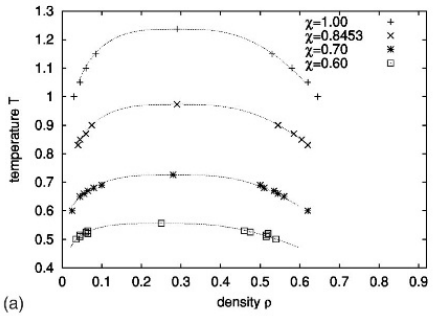

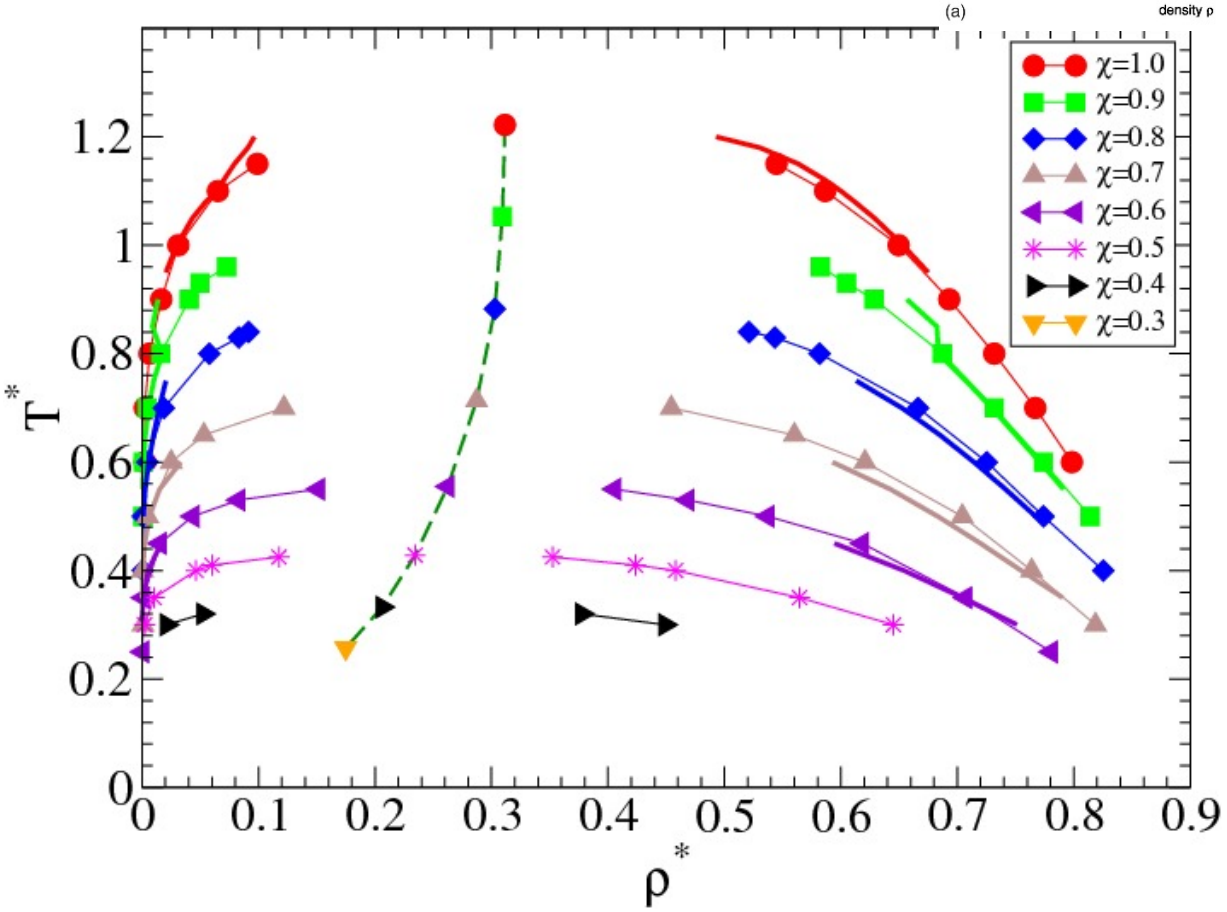

Giacometti, Lado, Largo, Pastore, Sciortino JCP 132 174110 (2010)

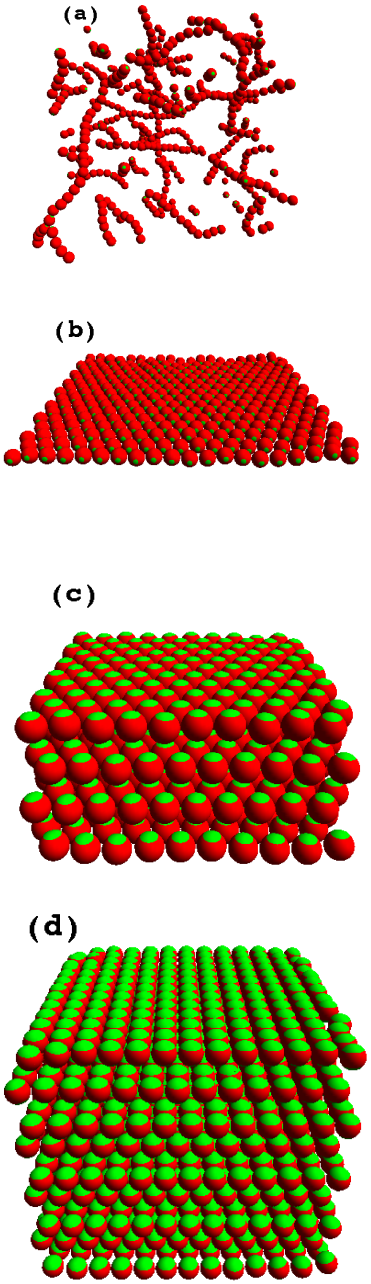

Characteristic configurations

Erdmann, Kroger, Hes, PRE 67, 041209 (2003)

1. nn-ss

$$\pm\hat{\mathbf{r}}_{12} = \hat{\mathbf{n}}_1 = -\hat{\mathbf{n}}_2$$

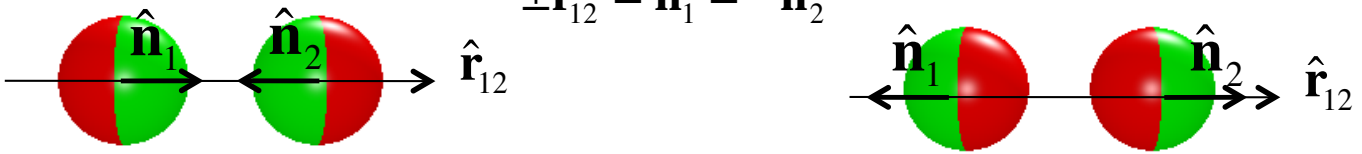

2. sn-ns

$$\pm\hat{\mathbf{r}}_{12} = \hat{\mathbf{n}}_1 = \hat{\mathbf{n}}_2$$

3. ee-ēē

$$\hat{\mathbf{r}}_{12} \perp \hat{\mathbf{n}}_1 = \pm\hat{\mathbf{n}}_2$$

4. es-en

$$\pm\hat{\mathbf{r}}_{12} = \hat{\mathbf{n}}_1 \perp \hat{\mathbf{n}}_2$$

Characteristic configurations

1.H-H

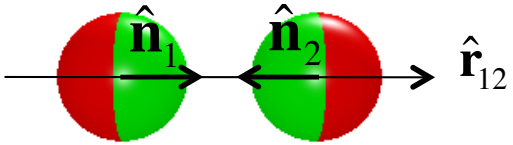

$$\pm\hat{\mathbf{r}}_{12} = \hat{\mathbf{n}}_1 = -\hat{\mathbf{n}}_2$$

2. H-T

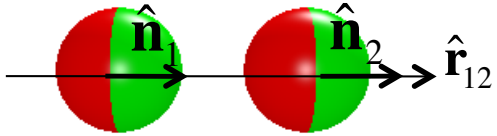

$$\pm\hat{\mathbf{r}}_{12} = \hat{\mathbf{n}}_1 = \hat{\mathbf{n}}_2$$

3. X

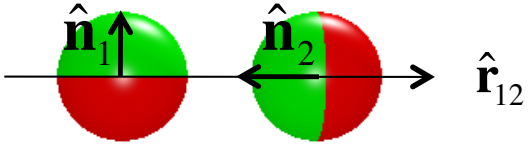

$$\pm\hat{\mathbf{r}}_{12} = \hat{\mathbf{n}}_1 \perp \hat{\mathbf{n}}_2$$

Correlation functions IE vs. MC

$$g(\mathbf{r}_{12},\hat{\mathbf{n}}_1,\hat{\mathbf{n}}_2) = 4\pi \sum_{l_1 l_2 l} \sum_{m_1 m_2} g(l_1 l_2 l, r) C(l_1 l_2 l, m_1 m_2 m_1 + m_2) Y_{l_1 m_1}(\omega_1) Y_{l_2 m_2}(\omega_2) Y^*_{l m_1 + m_2}(\Omega)$$

$$g(r,\omega_1,\omega_2) \qquad \bar{g}(r,\cos\theta_{12}) = \frac{1}{4\pi}\int d\Omega g(\mathbf{r}_{12},\hat{\mathbf{n}}_1,\hat{\mathbf{n}}_2) \qquad \bar{g}(\theta,\theta_2) = \frac{1}{(\lambda-1)\sigma}\int_{\sigma}^{\lambda\sigma} dr \left\langle g(\mathbf{r}_{12},\mathbf{n}_1,\mathbf{n}_2)\right\rangle_{\varphi\varphi_2}$$

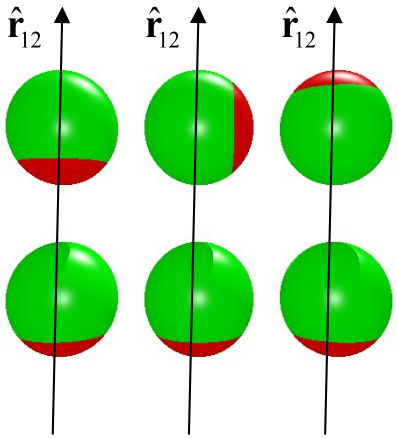

HT X HH

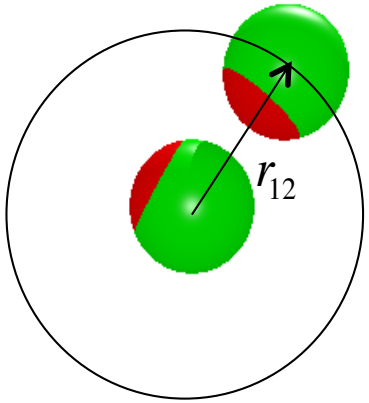

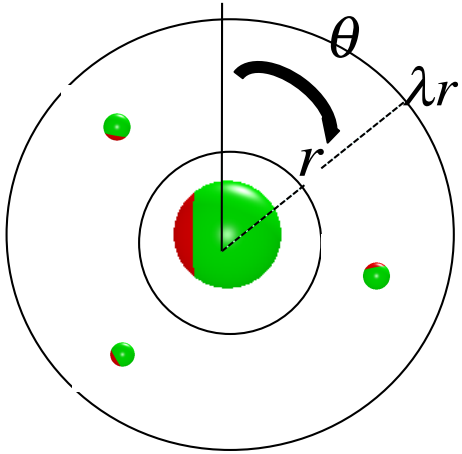

$$h^{l_1 l_2 l}(r)$$

projection over rotational invatiants

Giacometti, Lado, Largo, Pastore, Sciortino JCP 131, 174114 (2009)

Effect of coverage (2P)

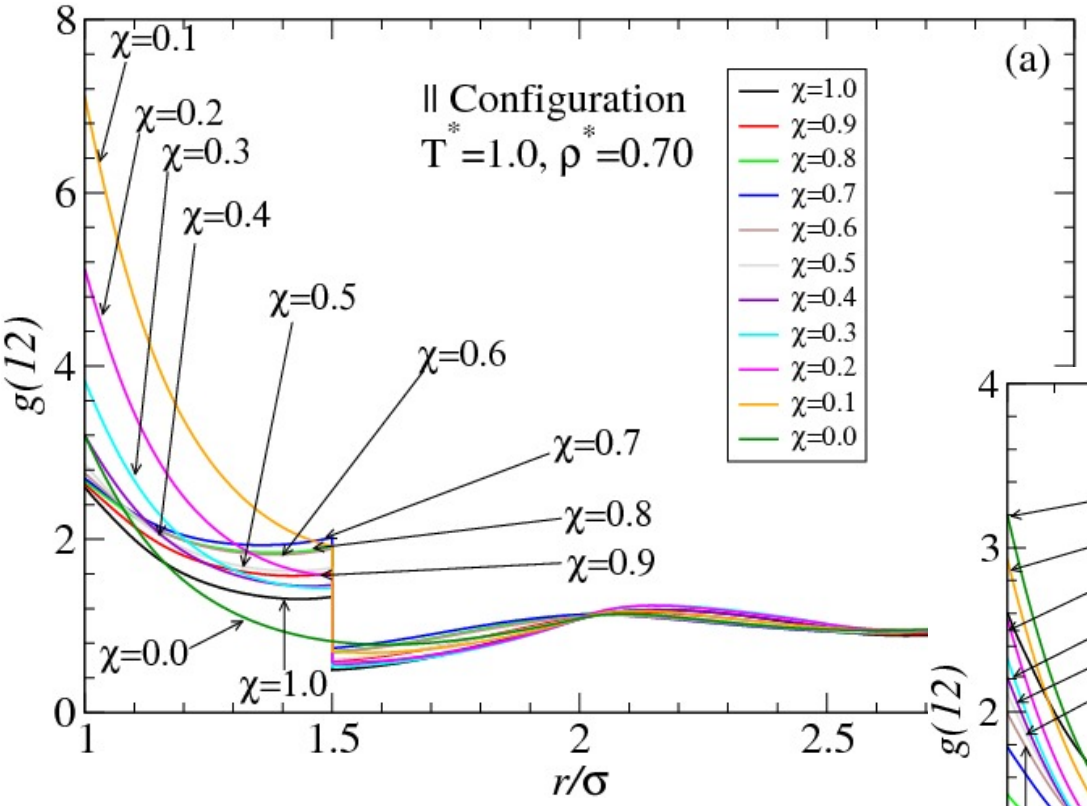

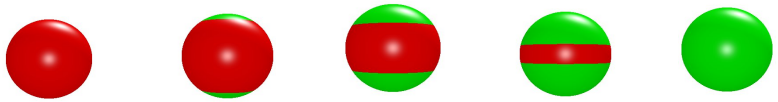

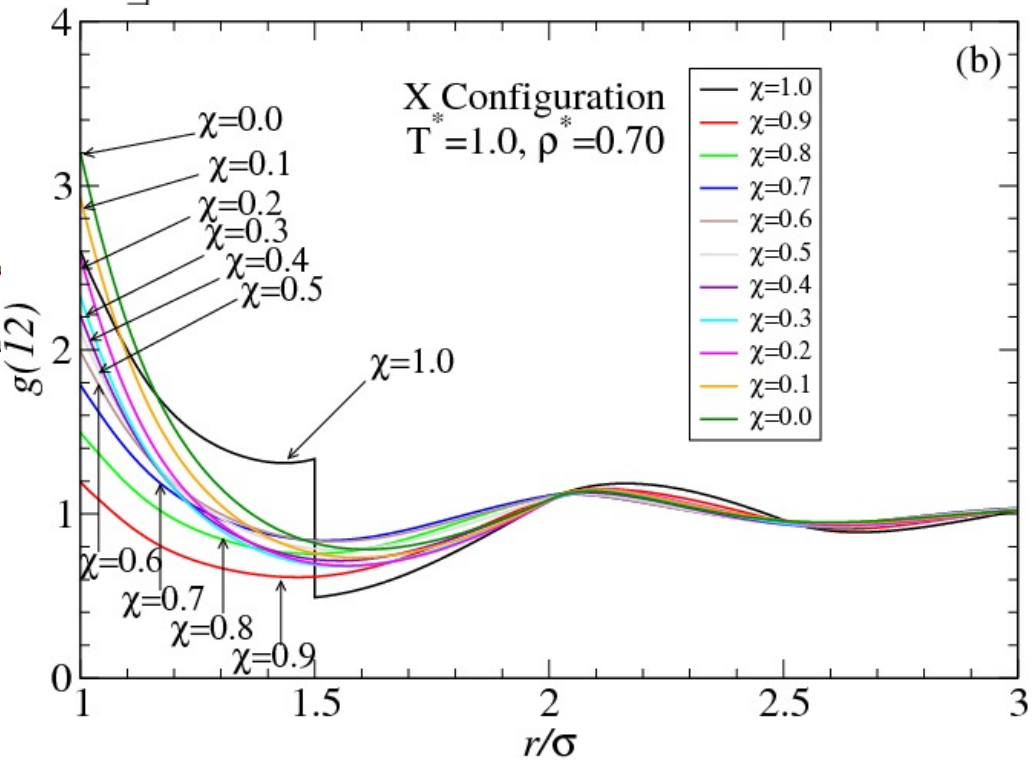

Giacometti, Lado, Largo, Pastore, Sciortino JCP 132 174110 (2010)

Angular average (2P)

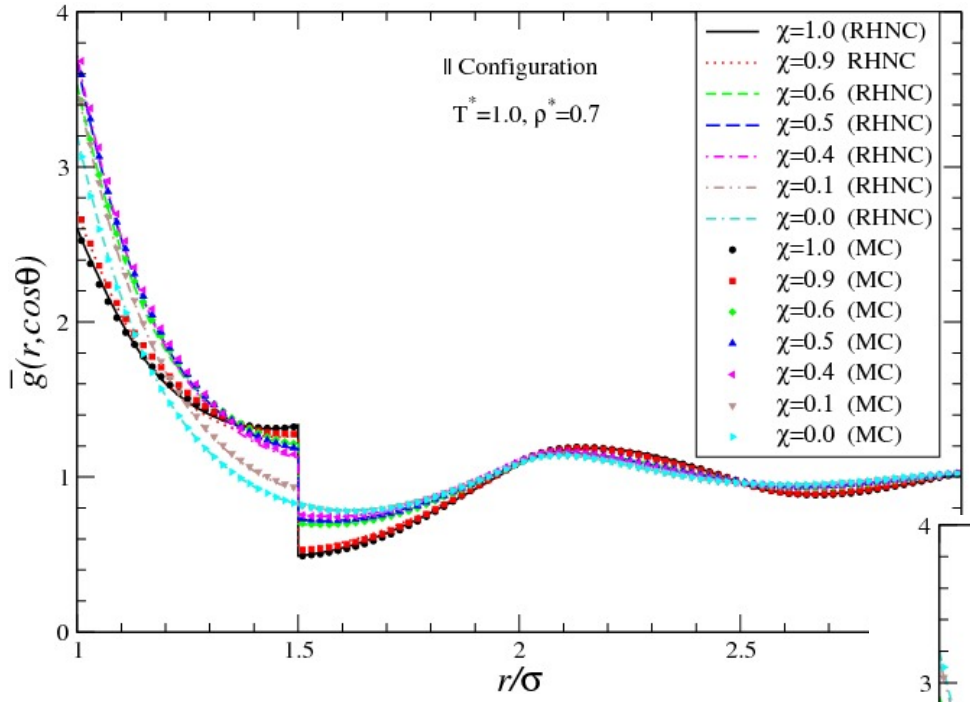

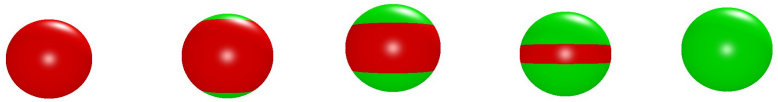

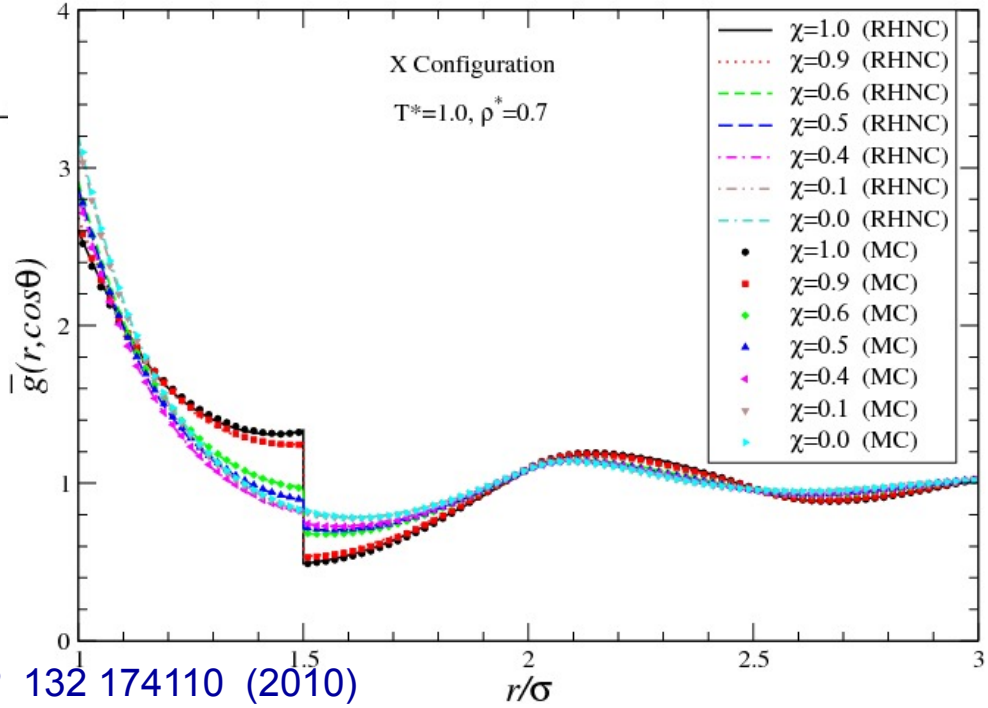

Giacometti, Lado, Largo, Pastore, Sciortino JCP 132 174110 (2010)

Effect of patch size and number

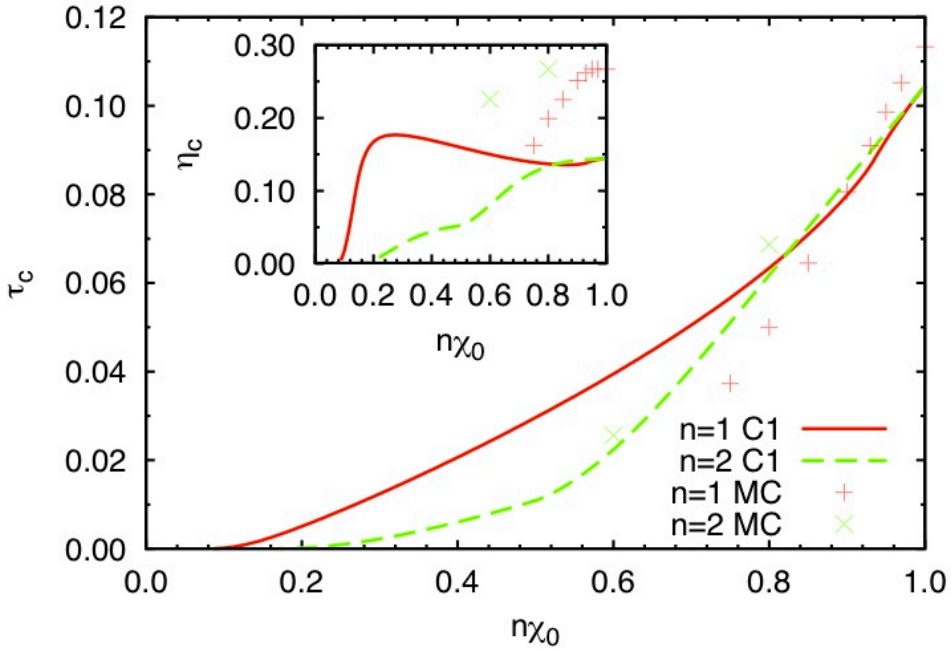

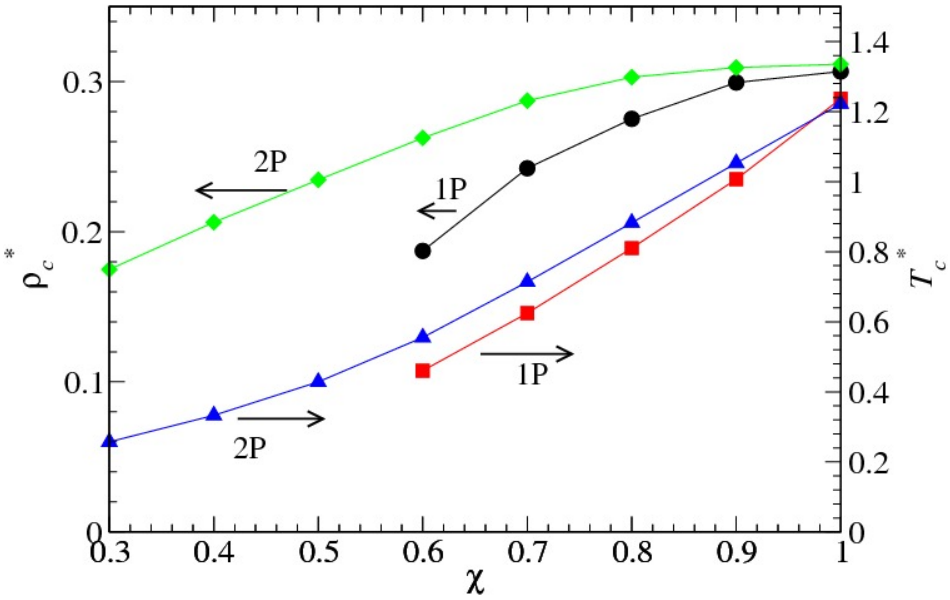

Fantoni, Gazzillo, Giacometti, Miller, Pastore,
JCP 127, 4507 (2007)

Giacometti, Lado, Largo,
Pastore, Sciortino JCP 132 174110 (2010)

UNIVERSITÀ CA' FOSCARI VENEZIA

Summary and outlook

Summary

- Anomalous phase diagram Janus fluid (Kern-Frenkel model)
- Estension to patchy (single and double) fluid
- Effect of patch size and number
- Integral equation theory good agreement

Outlook

- Role of the interaction range
- Stability of the algorithm for integral equations
- Theory of non-interacting clusters
- Applications to DNA


Università
Ca'Foscari
Venezia
Thank you for your attention!

Entropy balance

Sciortino, Giacometti, Pastore, PRL 103, 237801 (2009)

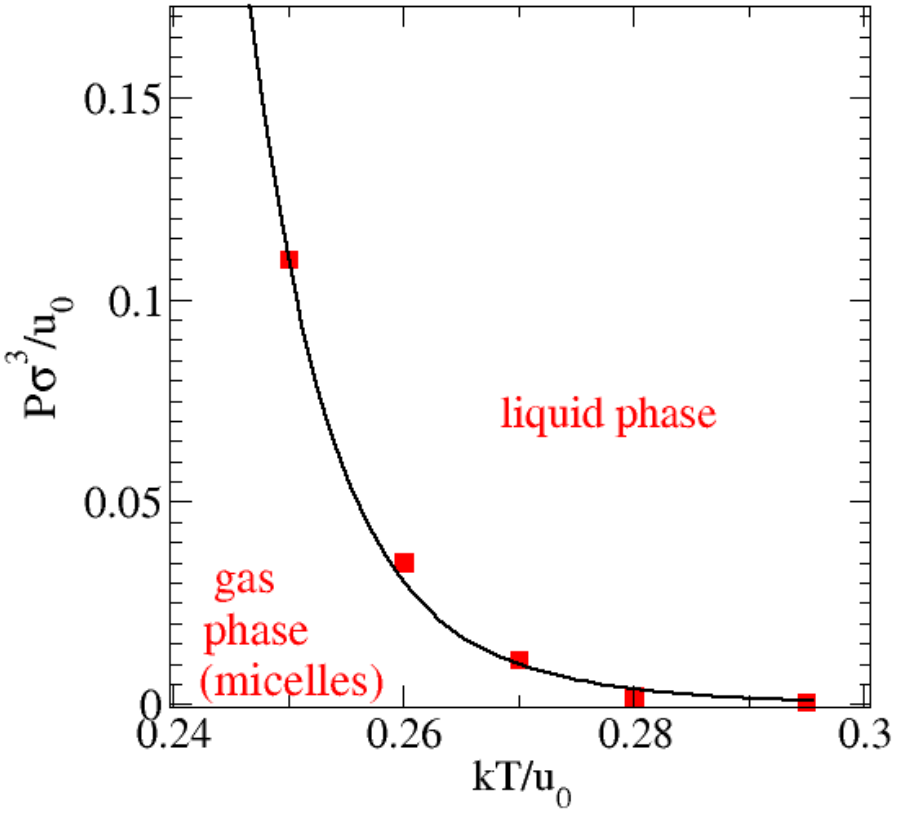

$$\left(\frac{dP}{dT}\right) = \frac{\Delta S}{\Delta V} < 0$$

$$V_g > V_l \Rightarrow S_g < S_l$$

Gas phase has lower entropy than liquid phase!

Energy vs entropy balance

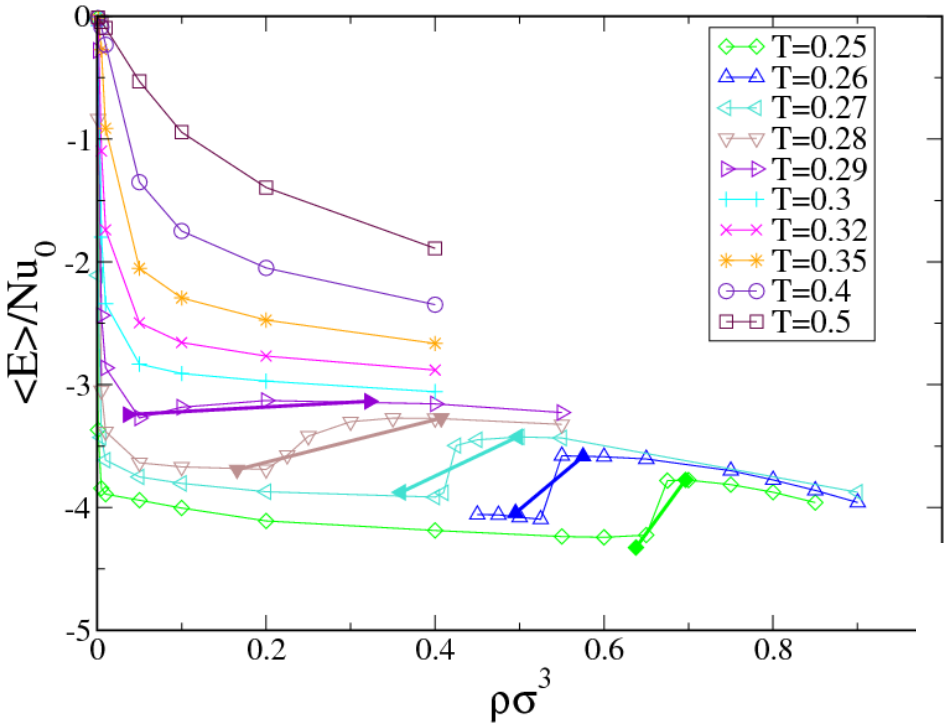

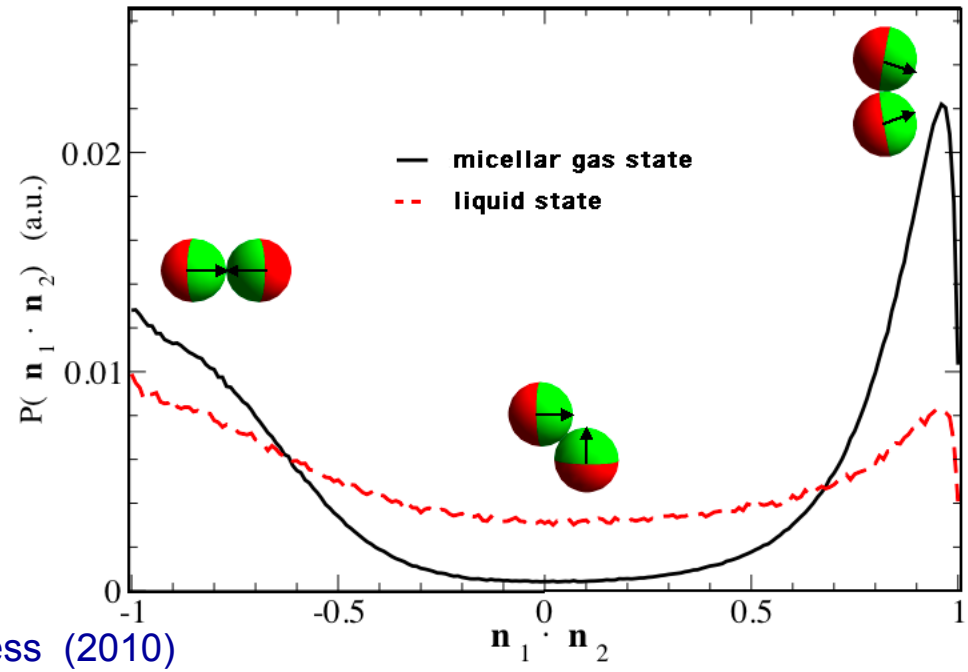

Energy of the gas phase lower than liquid phase

Entropy gas phase lower than liquid phase

Sciortino, Giacometti, Pastore PCCP in press (2010)

Role of the range interaction

Letters Langmuir, Vol. 24, No. 3, 2008 623

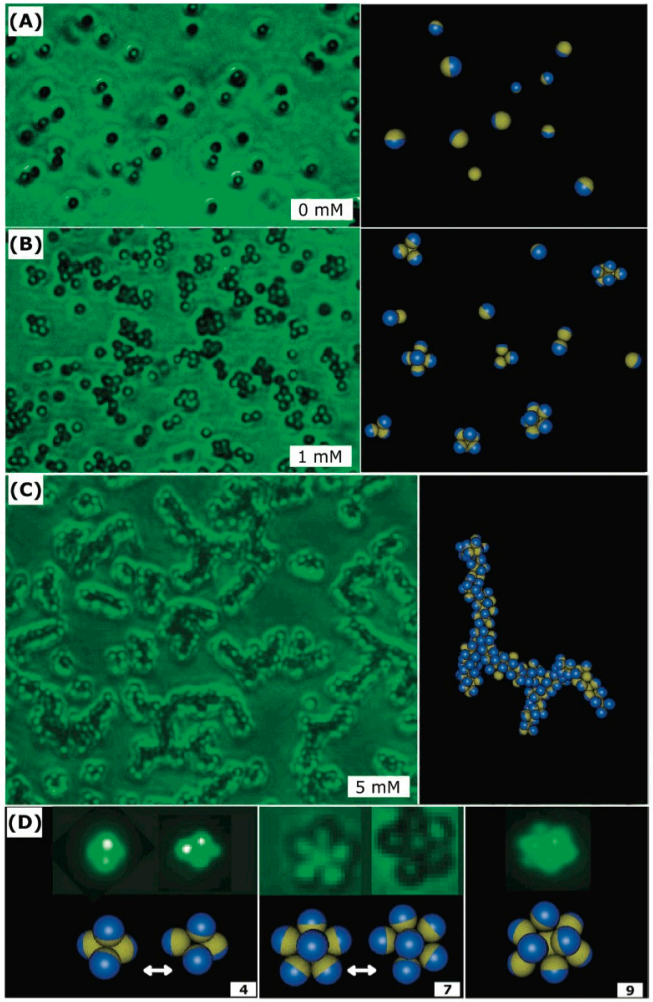

Figure 3. Varying the salt concentration causes amphiphilic particles (1 μm diameter) to assemble into clusters of various sizes and shapes. The images with green background represent epifluorescence experiments. In the Monte Carlo computer simulations, blue and yellow colors represent charged and hydrophobic hemispheres, respectively. Panel (A) shows discrete particles for the case of particles in deionized water. Panel (B) (1 mM KNO_3) shows small clusters (up to nonahedra) in equilibrium with one another. Panel (C) (5 mM KNO_3) shows long, branched wormlike strings. The simulations (right) confirm that the assembly of small clusters into strings occurs as the range of the electrostatic repulsion, relative to hydrophobic attraction, decreases with increasing salt. Panel (D) shows further comparison of epifluorescence images and Monte Carlo simulations with excellent agreement. Experimentally, clusters with the same number of particles (N) interconvert dynamically between different shapes, as confirmed from simulations for tetramers, $N = 4$ (left), and heptamers, $N = 7$ (middle). The nonahedral structure, $N = 9$, is also confirmed (right).

Why are we not observing spiral-like clustering?

1. KF model comparable only in the limit of high salt concentration
2. Range of interaction is different

Experimental range 0.1σ

Simulation range 0.5σ

- Lower ranges requires bigger computational effort
- Experimental range could be tuned using Casimir effect

Gambassi et al, Europhys. News 40, 18 (2009)

Hong, Cacciuto, Luijten, Granick, Langmuir 24, 621 (2008)

Additional evidence

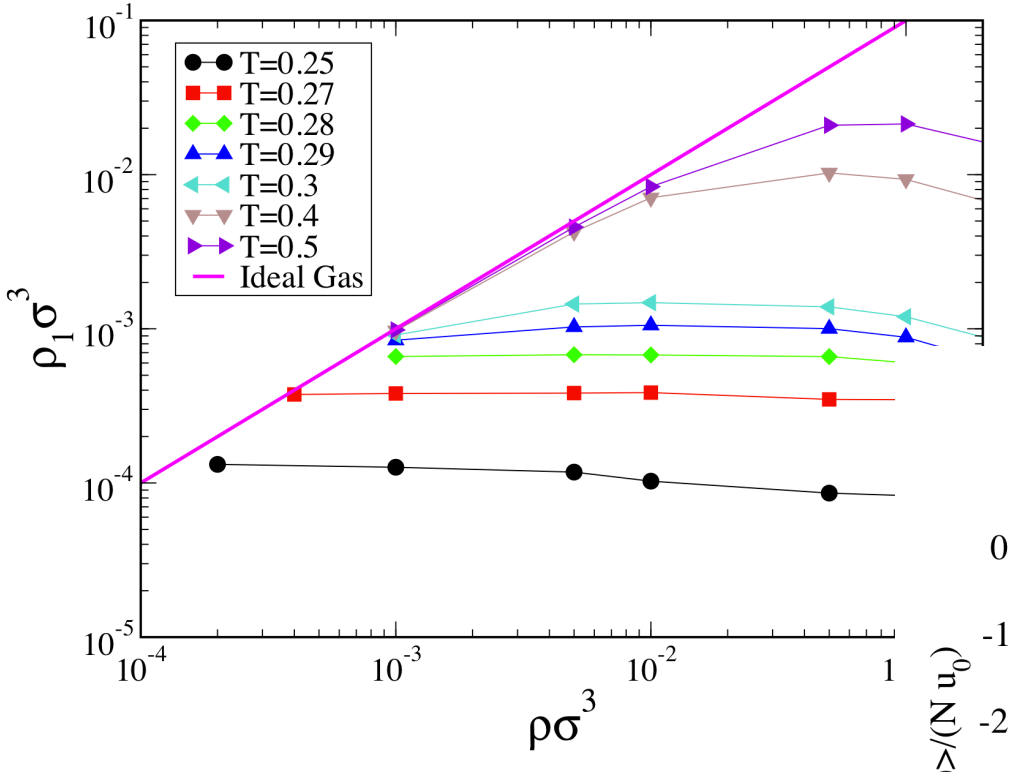

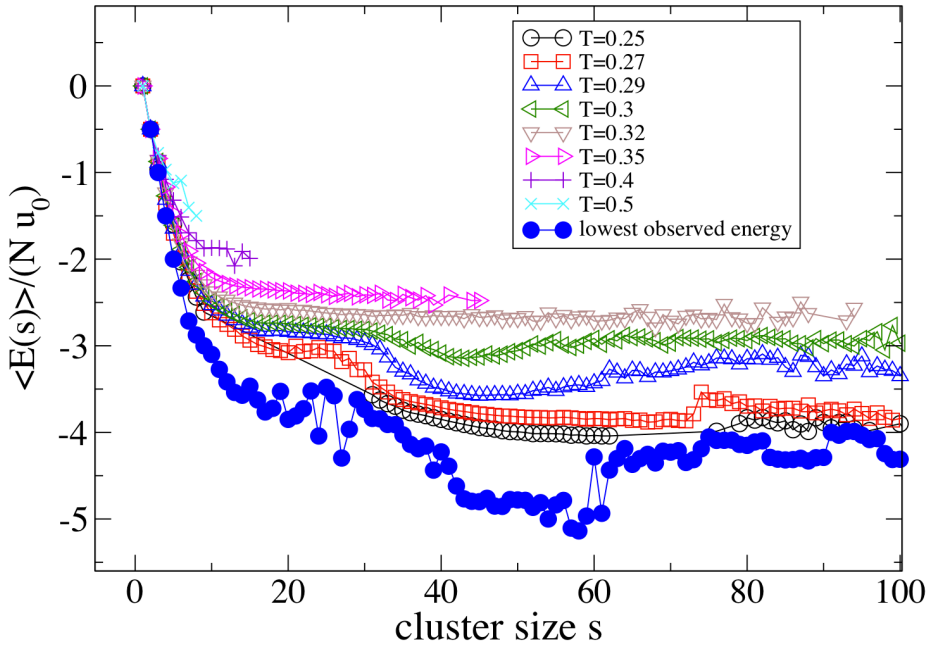

Note that the average energy of a given cluster size is,
to good approximation, independent of density, so clusters are not interacting (ideal gas)

Details of the simulations

0.1σ $0.1rad$

MC sweep= attempted random translation and random rotation of each particle

Coexistence lines: GEMC simulations $N = 350$ $V = 2868\sigma^3$

$\rho\sigma^3 = 0.122$

Lowest considered temperature $N_l = 320$ $V_l \approx 8\sigma$

Equilibration CPU time ≈1 month $N_g = 30$ $V_l \approx 13\sigma$

Critical point: GCMC simulations + histogram reweighted techniques $L = 15\sigma$

Structural properties: NVT simulations $N = 5000$ $V = 3775\sigma^3$

Equilibration time: 10^9 steps

Clausius-Clapeyron equation: NPT simulations

Method for coexisting curve

$$P(\rho_l) = P(\rho_g)$$

$$\mu(\rho_l) = \mu(\rho_g)$$

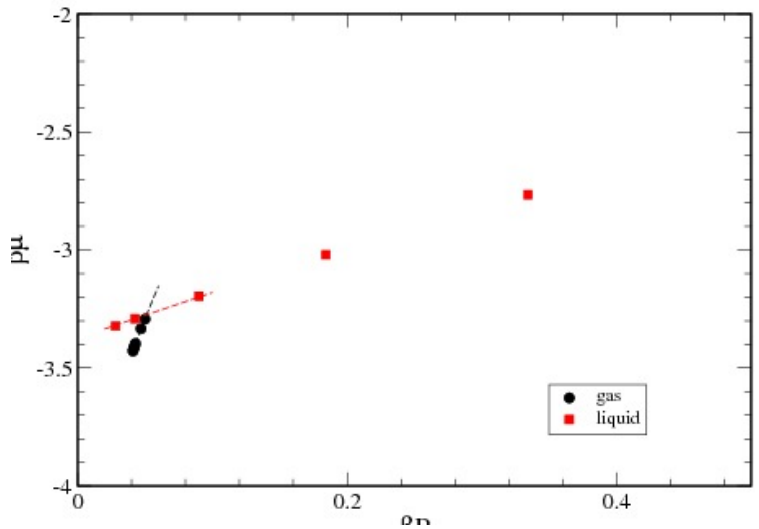

- Start two calculations from low and high density
- Look for the numerical solution of the non-linear set of equation

RHNC closure: good and bad issues

☺

- Only a single approximation at level of B(r)
- Simple to use (also for patchy system)
- Well defined theoretical ground
- Gives rather precise predictions

☹

- No true critical point
- Difficult to improve

$$\rho \frac{\partial}{\partial \rho}\left(\frac{\beta U}{N}\right) = \beta \frac{\partial}{\partial \beta}\left(\frac{\beta P}{\rho}\right)$$

Hiroike's condition for internal consistency

What about the discontinuity?

The particular factorization form of the potential allows Φ(12) to remain unexpanded

1. Evaluate χ by Gauss-Legendre quadratures using n roots

$$\chi^2 = \left\langle \Psi\left(\hat{\mathbf{n}}_1, \hat{\mathbf{n}}_2, \hat{\mathbf{r}}_{12}\right)\right\rangle_{\omega_1\omega_2}$$

2. Compare it with exact result $\chi = \sin^2 \frac{\theta_0}{2}$

3. Use optimal n in all further calculations (typically n=30-40)

Ex: $$\frac{\beta U}{N} = -2\pi\rho\beta\varepsilon \int_{\sigma}^{\lambda\sigma} dr r^2 \left\langle g\left(r, \omega_1, \omega_2\right)\Psi\left(\omega_1, \omega_2\right)\right\rangle_{\omega_1\omega_2}$$

Note: Expansion in spherical harmonics terminated at $l_1 = l_2 = m = 4$

35 distinct coefficients

UNIVERSITÀ CA' FOSCARI VENEZIA

Corresponding State principle?

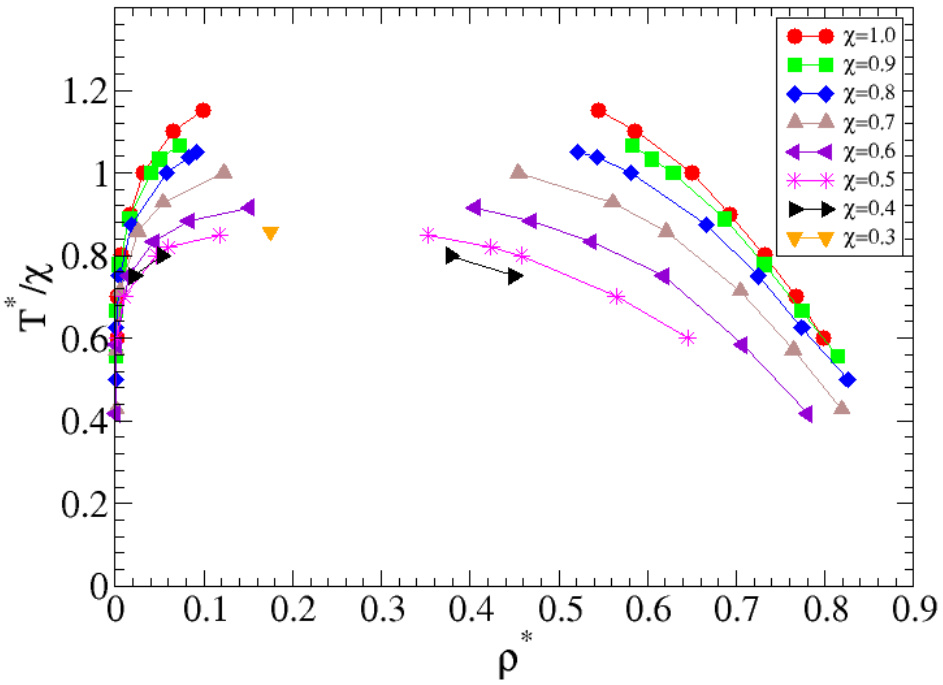

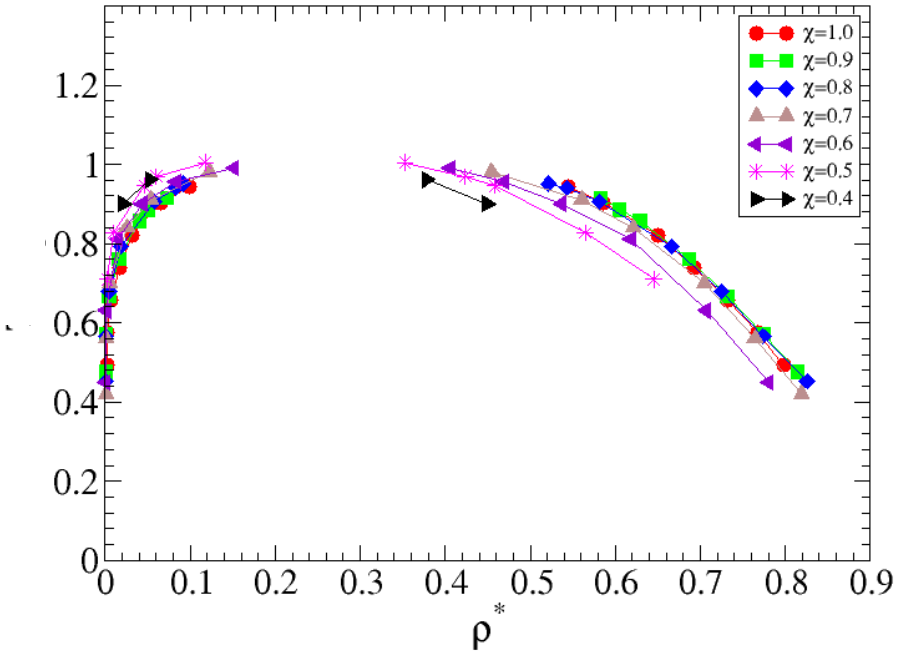

UNIVERSITÀ CA' FOSCARI VENEZIA

Cluster free energies

$$\frac{\beta F}{V} = \sum_n \left[\rho_n \log(\Lambda \rho_n^3) - \rho_n \right] + \sum_n \rho_n \beta \phi_n$$

$$\beta \mu_n = \frac{\partial}{\partial \rho_n} \left(\frac{\beta F}{V} \right) = \log\left(\rho_n \Lambda^3 \right) + \beta \phi_n$$

Equilibrium conditions $\mu_n = n \mu_1$

Free energy of the n-th cluster (with n particles)

$$\phi_n = n \phi_1 + k_B T \log \left[\frac{\rho_n \Lambda^3}{\left(\rho_1 \Lambda^3 \right)^n} \right]$$

UNIVERSITÀ CA' FOSCARI VENEZIA

Percolation

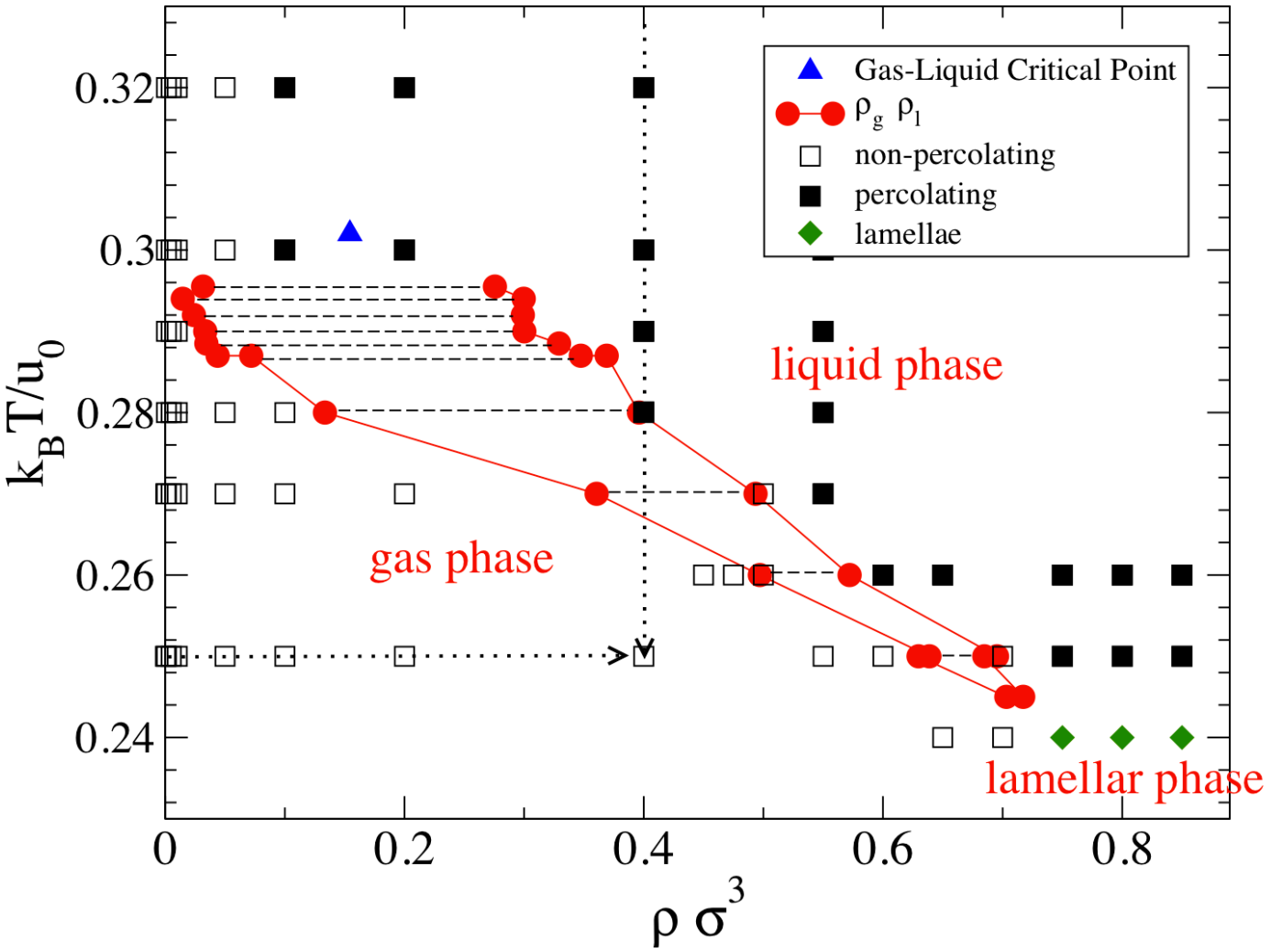

UNIVERSITÀ CA' FOSCARI VENEZIA

Cluster distribution